Journal of Applied Electrochemistry **29**: 637–645, 1999.

Microstructural characterization and corrosion resistance of Ni–Zn–P alloys electrolessly deposited from a sulphate bath

M. BOUANANI[1], F. CHERKAOUI[1], R. FRATESI[2]*, G. ROVENTI[2] and G. BARUCCA[3]
[1]*Laboratoire d'Electrochimie et de Chimie Analytique, Faculté des Sciences, Université Mohammed V. Avenue Ibn Battouta B.P. 1014, Rabat, Morocco;*
[2]*Dipartimento di Scienze dei Materiali e della Terra,*
[3]*INFM Università degli Studi di Ancona, Via Brecce Bianche 60131, Ancona, Italy*
*(*author for correspondence)*

Received 27 July 1998; accepted in revised form 11 November 1998

Key words: alloys, electroless, microstructure, morphology, nickel, phosphorus, zinc

Abstract

Electroless Ni–Zn–P alloy coatings were obtained on an iron substrate from a sulfate bath at various pH values. The effects of changes in bath pH on alloy composition, morphology, microstructure and corrosion resistance were studied. Scanning electron microscopy was performed to observe the morphological change of the deposits with bath pH. Coating crystallinity was investigated by grazing incidence asymmetric Bragg X-ray diffraction and transmission electron microscopy. A transition from an amorphous to polycrystalline structure was observed on increasing the bath alkalinity, and thus decreasing the phosphorus content of the alloys. A single crystalline phase corresponding to face-centred-cubic nickel was identified in the alloys obtained from a strong alkaline solution. An increase in zinc percentage up to 23% in the deposits does not change the f.c.c. nickel crystalline structure. Corrosion potential and polarization resistance measurements indicated that the corrosion resistance of electroless Ni–Zn–P alloys depends strongly on the microstructure and chemical composition. The deposits obtained at pH 9.0–9.5 and with 11.4–12.5% zinc and 11.8–11.2% phosphorous exhibited the best corrosion resistance.

1. Introduction

The increasing demand for corrosion resistant coatings has led researchers to study new materials. In particular, metallic coatings containing nonmetallic element inclusions such as phosphorous have received considerable attention; in fact it was found that the addition of phosphorous to the iron group metals or their alloys strongly affects the physico-chemical properties [1].

Nickel–phosphorous binary alloys are well known for their good corrosion resistance, mechanical properties and magnetic effects. These alloys can be produced by electrodeposition [2–4] or by electroless deposition [5–12] and their properties are strongly dependent on the preparation process [13]. Microstructural investigations of as-deposited electroless Ni–P alloys showed contradictory results: some authors [9, 11, 12] found amorphous, liquid-like structures, whereas Graham et al. [10] found a polycrystalline structure with fine grain size, corresponding to the face-centred cubic (f.c.c.) structure of nickel. This difference was explained by the different sample preparation [12]. Chow et al. [14] confirmed the f.c.c. structure of nickel for Ni–P films electrolessly deposited from strong alkaline solution.

The ternary Ni–Zn–P alloys have been less investigated. The phosphorous addition to the electrodeposition bath of zinc–nickel alloys was found to refine the microstructure and improve the corrosion resistance of the deposits [15]. Composition, morphology and corrosion resistance of Ni–Zn–P alloy coatings (Zn 13.3–75.1%, P 5.9–0.4%), obtained by electrodeposition from chloride bath at a rotating cylinder electrode, have been studied by Swathirajan and Mikhail [16]. Recently the electroless deposition of Zn–Ni–P alloys rich in zinc was proposed to provide a sacrificial, corrosion-protective coating, which may be applied after assembly of components and which is compatible with subsequent operations such as painting [17]. Electroless deposition

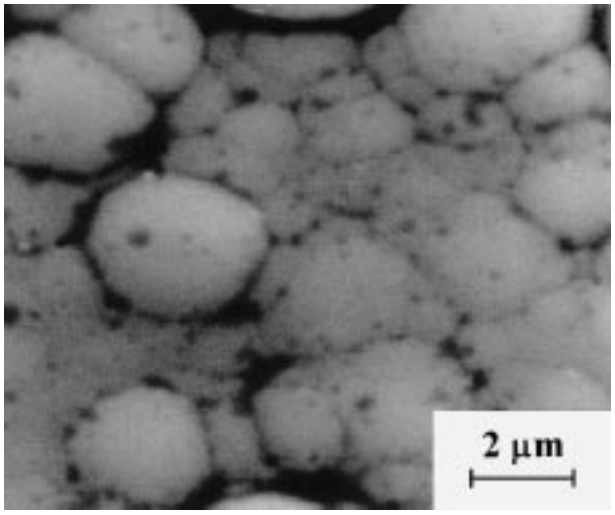

Fig. 1. Scanning electron image of a $Ni_{76.8}$–$Zn_{11.4}$–$P_{11.8}$ deposit obtained from the basic bath (pH 9.0).

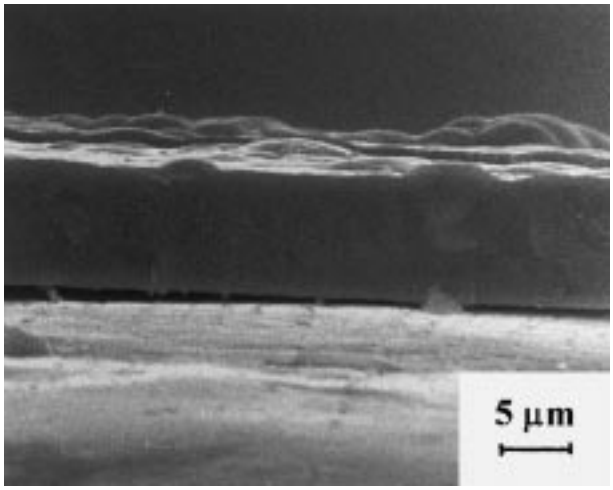

Fig. 3. Scanning electron micrograph of a cross section of the deposit obtained from the basic bath.

of Ni–Zn–P thin films from a chloride bath on an $SnCl_2$–$PdCl_2$ activated substrate has been studied by Schlesinger et al. [18, 19]. The films had a high nickel content and very small crystallite sizes; the authors evaluated the roles of microstructure in determining and controlling corrosion properties.

Previously, we investigated the effect of the different plating parameters (T, pH and $[Zn^{2+}]$) on the composition and the plating rate of Ni–Zn–P alloys rich in Ni, electrolessly deposited from a sulphate bath on Armco iron sheets [20]. In the present work the effects of changes in morphology, microstructure and corrosion resistance of the alloy coatings with the pH of the bath were studied. Morphological and microstructural analyses of the deposits were performed by scanning (SEM) and transmission (TEM) electron microscopy techniques and grazing incidence asymmetric Bragg X-ray diffraction (GIABD). The corrosion behaviour was studied by corrosion potential (E_{corr}) and polarization resistance (R_p) measurements performed in quiescent aerated 3% NaCl solution.

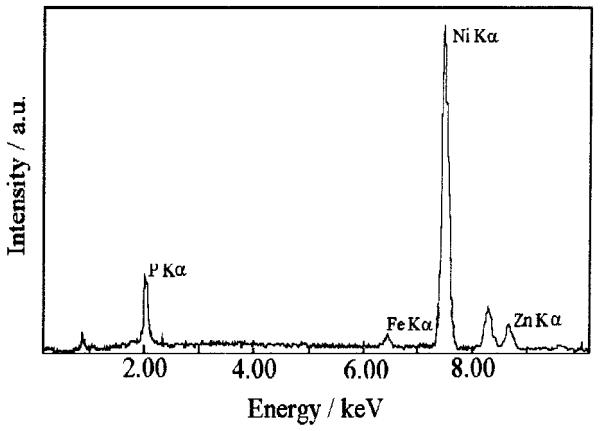

Fig. 2. X-ray microanalysis of the deposit obtained from the basic bath.

2. Experimental details

Ni–Zn–P alloys were electrolessly deposited at 90 °C from a basic bath of the following composition: $NiSO_4.6H_2O$ 27 g dm^{-3} (0.1 M); $ZnSO_4.7H_2O$ 2.9 g dm^{-3} (0.01 M); $NaH_2PO_2.H_2O$ 32 g dm^{-3} (0.3 M); $C_6H_5Na_3O_7.2H_2O$ 59 g dm^{-3}; $(NH_4)_2SO_4$ 27 g dm^{-3} and lactic acid 10 g dm^{-3}. The pH was adjusted to 9.0 by addition of sodium hydroxide. To study the effects of bath pH on the physico-chemical properties of the alloys, some depositions were performed at pH between 8.0 and 11.2; pH was changed by addition of sodium hydroxide. All the solutions were prepared with doubly distilled water and analytical grade reagents and were deaerated by nitrogen bubbling. Electroless deposits were obtained on Armco iron sheets (exposed area 3 cm^2), which were mechanically polished with progressively finer grades of emery paper, chemically etched in dilute sulphuric acid and rinsed with distilled water before the experiments. After deposition, the samples were washed with distilled water and dried with hot air.

The composition of the deposits was determined using an inductively coupled plasma spectrometer (Perkin Elmer Optima 3200 XL) and a energy dispersive X-ray spectrometer (Edax PV9800). Scanning electron micros-

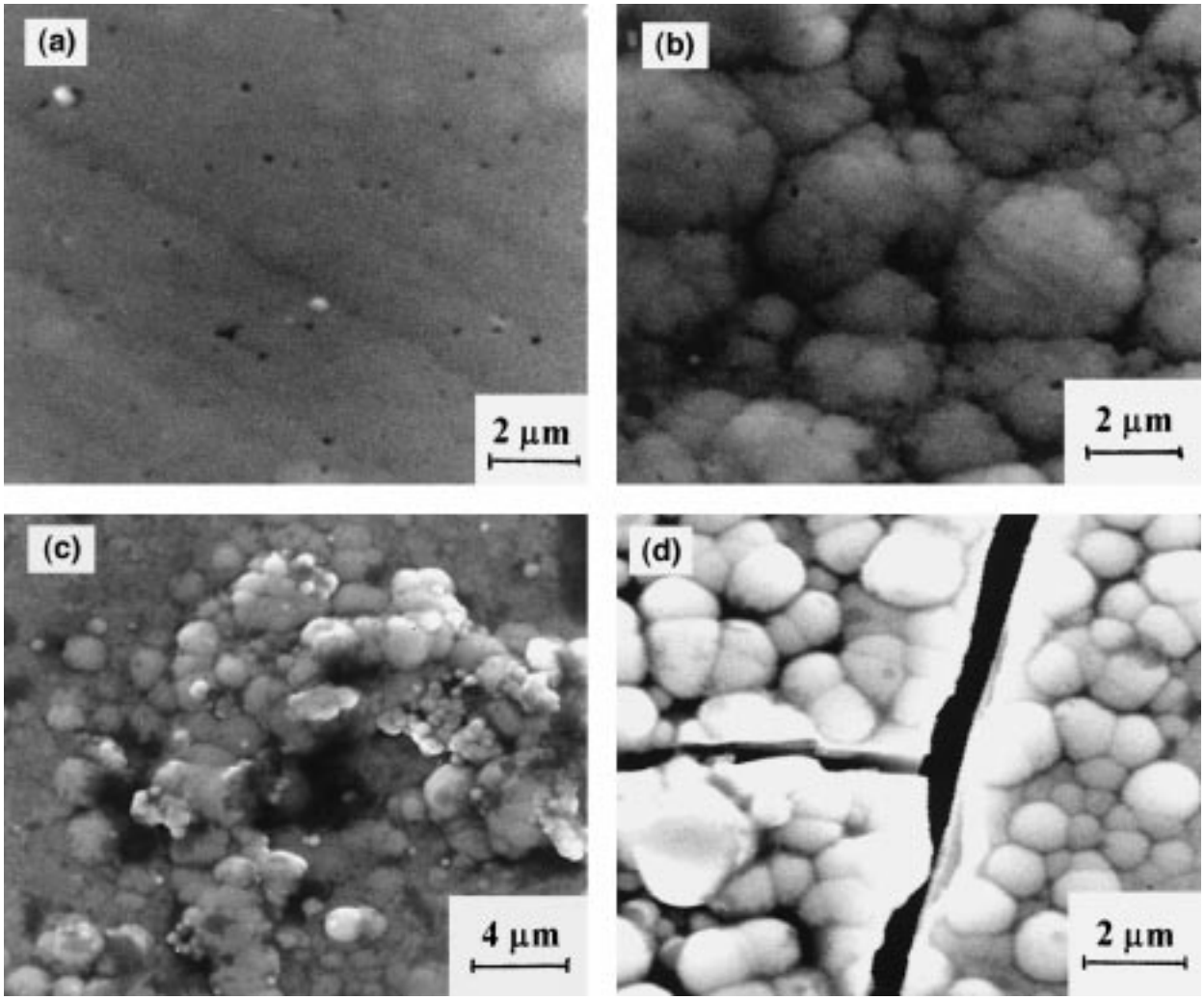

Fig. 4. Scanning electron images of the deposits obtained at different bath pH. (a) pH 8.0, Ni_{79}–$Zn_{8.5}$–P_{13}; (b) pH 9.5, $Ni_{76.3}$–$Zn_{12.5}$–$P_{11.2}$; (c) pH 10.0, $Ni_{79.8}$–$Zn_{13.3}$–P_7 and (d) pH 11.2, $Ni_{83.6}$–Zn_{10}–P_5.

copy to study the surface and the cross-section morphology was performed on a Philips XL 20 instrument. The cross sections were obtained by fracture of the samples in liquid nitrogen, in order to avoid modifications of the coating structure. Grazing incidence asymmetric Bragg X-ray diffraction spectra were acquired using a INEL CPS 120 diffractometer with CuK_α radiation (1.540 56 Å). Transmission electron microscopy was performed on a Philips CM 200 instrument. The samples were prepared for TEM observations by conventional techniques and the final thinning was carried out in an ion beam using Ar^+ ions at 5.5 kV, 0.5 mA and an incidence angle of 14°. During this stage the specimens were continuously cooled by liquid nitrogen to prevent any possible changes induced by warming. Deposits which did not adhere on the iron sheet were peeled off and ground to reduce their thickness before the TEM observation.

The corrosion behaviour of electroless Ni–Zn–P alloys was studied by corrosion potential (E_{corr}) and polarization resistance (R_p) measurements carried out in quiescent aerated 3% NaCl solution. The experiments were performed using a EG&G Princeton Applied Research (PAR) model 273 potentiostat/galvanostat and a PC with the m352 corrosion software. The auxiliary electrode was a platinum spiral and the reference electrode was a saturated calomel electrode (SCE). On immersion, the corrosion potential was measured and recorded against time until its change was less than $10\,mV\,h^{-1}$. The polarization resistance was then measured by potentiodynamic polarization at $0.2\,mV\,s^{-1}$ from 15 mV cathodic to 15 mV anodic of E_{corr}. The R_p value was calculated from the slope of the curve.

3. Results and discussion

3.1. *Deposit morphology*

The Ni–Zn–P deposit obtained from the basic bath is bright grey in appearance; SEM observation shows that its surface morphology is homogenous and not porous, with rounded formations (Fig. 1). From the energy dispersive X-ray analyses (EDX) it was found that the chemical composition is almost the same in the different zones. The percentages in weight of the deposit elements are 11.4% zinc, 11.8% phosphorus and 76.8% nickel. Figure 2 shows a typical EDX spectrum where only the Ni, Zn, P and Fe elements appear, demonstrating the purity of the coating; the Fe peak is due to substrate interference. SEM observation on the cross sections of this coating showed that the deposit develops in a uniform fashion on the substrate (Fig. 3).

To analyse the effect of solution pH on the composition and surface morphology, some depositions were carried out from baths of different pH (8.0, 9.5, 10.0 and 11.2). All the deposits were bright or semibright grey. Figure 4 shows the SEM images of the Ni–Zn–P alloys. A gradual morphological change with pH is clearly visible: the coating obtained from pH 8.0 is uniform, homogenous and smooth (Fig. 4(a)); when the pH increases, the coatings are also homogenous and uniform, but show rounded formations (Figs 1, 4(b), (c) and (d)). At pH 11.2 (Fig. 4(d)), the deposit is cracked and does not adhere to the iron substrate. The cracks in the deposits are generally due to internal stress which depends on several parameters such as the nature and state of the substrate, the composition of the deposit and hydrogen penetration during the deposition. The decrease in the phosphorus content in the deposit from 13% at pH 8 to 5% at pH 11.2 is the probable cause of the cracks, in agreement with other work on electroless Ni–P alloys [5], where it was found that the internal stress increases with decrease in deposit phosphorus content.

The deposits obtained at pH 9.5 and 10.0 with a zinc concentration in solution higher (Zn^{2+} 0.05 M) than that of the basic bath also have a phosphorus percentage of about 5%, but do not exhibit cracks (Figs 5(a) and (b)); their zinc content ranges between 18 and 23%. This fact indicates that a low phosphorus percentage in the deposit causes internal stress which is reduced by the higher percentage of zinc. The presence of cracks was also observed by other authors in Ni–Zn–P electrodeposits and was attributed to the internal stress caused by nickel lattice distortion [16]. Cracks due to a low content of zinc in the deposits were found also in Co–Zn alloys electrodeposits [21–23].

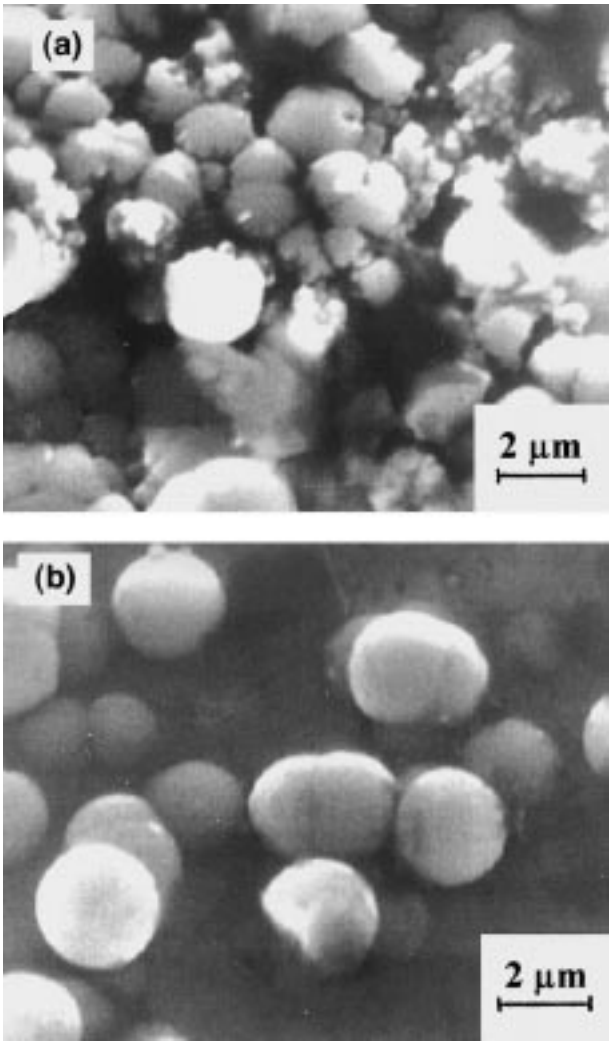

Fig. 5. Scanning electron images of the deposits obtained from a solution with 0.05 M in zinc. (a) pH 9.5, $Ni_{76.7}$–Zn_{18}–$P_{5.7}$; (b) pH 10.0, $Ni_{72.7}$–Zn_{23}–P_5.

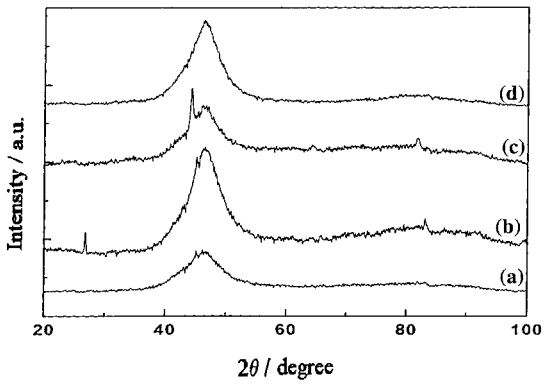

Fig. 6. X-ray diffraction patterns of Ni–Zn–P alloys deposited at different bath pH. (a) pH 8.0; (b) pH 9.0; (c) pH 10.0 and (d) pH 11.2.

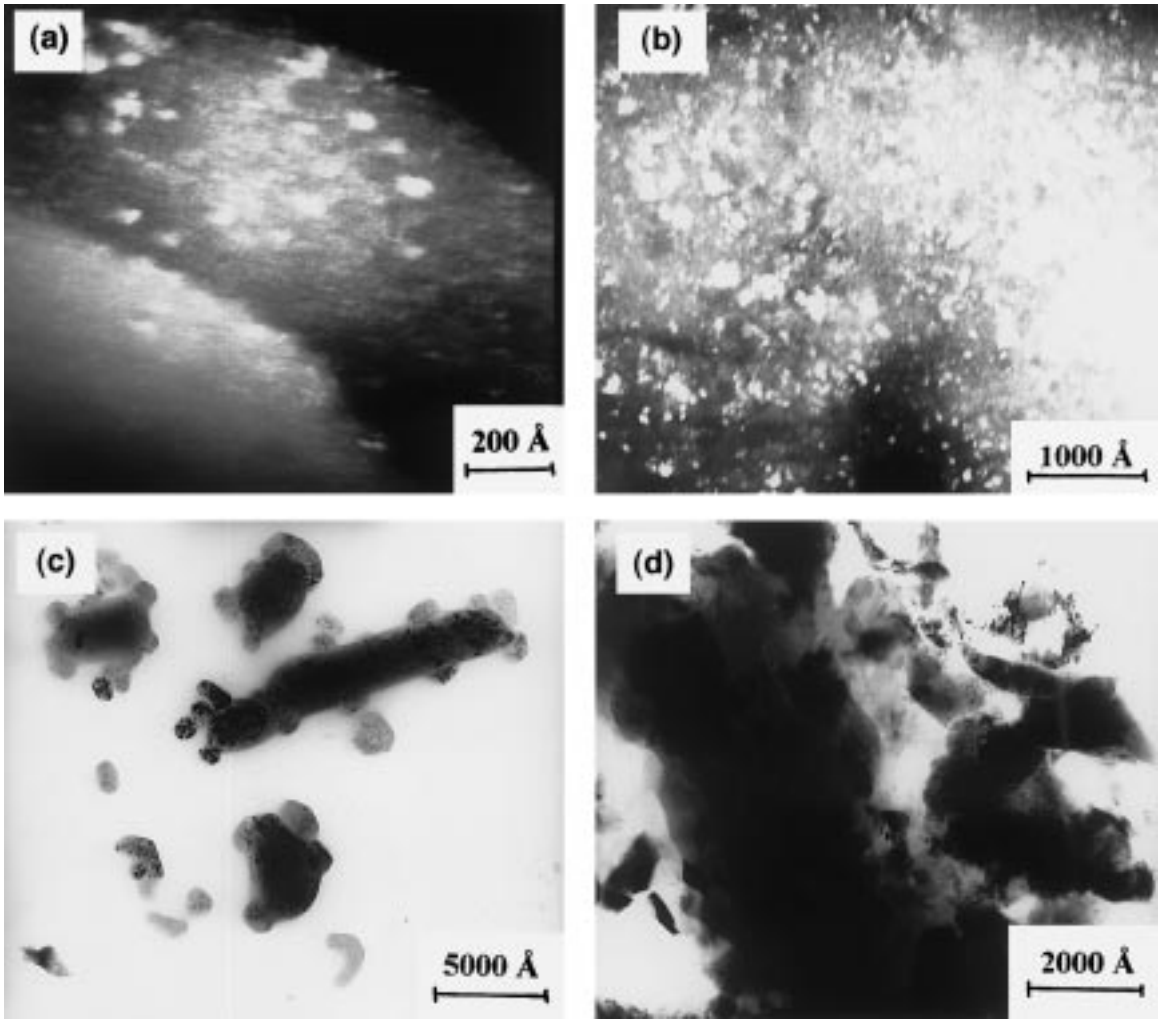

Fig. 7. TEM images of Ni–Zn–P alloys deposited from alkaline solutions. (a) pH 8.0, dark field; (b) pH 9.0, dark field; (c) pH 10.0, bright field; (d) pH 11.2, bright field.

3.2. *X-ray diffraction*

GIABD spectra of the electroless Ni–Zn–P alloys are reported in Figure 6. Only one broad peak is present in all the curves; the half-height width of this peak reduces on changing the pH from 8.0 to 11.2. The sharper peaks in curves (b) and (c) are linked to the iron substrate. The X-ray diffraction patterns suggest that in the Ni–Zn–P alloys an amorphous phase coexists with a crystalline one. On increasing the bath pH, the amount of crystalline phase increases with respect to the amorphous one.

GIABD analysis did not permit identification of the crystalline phase present in the alloys, therefore transmission electron microscopy was performed.

3.3. *TEM analyses*

Figure 7(a)–(d) shows TEM images of electroless Ni–Zn–P alloy deposits obtained from different alkaline baths (8.0, 9.0, 10.0 and 11.2).

The images show that the Ni–Zn–P alloy are made of crystallites uniformly distributed in an amorphous matrix. The size of the crystallites varies according to bath alkalinity. In particular, it ranges from about 65 Å for the alloy obtained at pH 8 (Fig. 7(a)) to 5000 Å for that deposited at pH 11.2 (Fig. 7(d)). Electron diffraction patterns corresponding to the different deposits are reported in Figure 8. The very broad rings, corresponding to the deposit obtained at pH 8.0 (Fig. 8(a)) become sharper at pH 9.0 (Fig. 8(b)). The electron diffraction

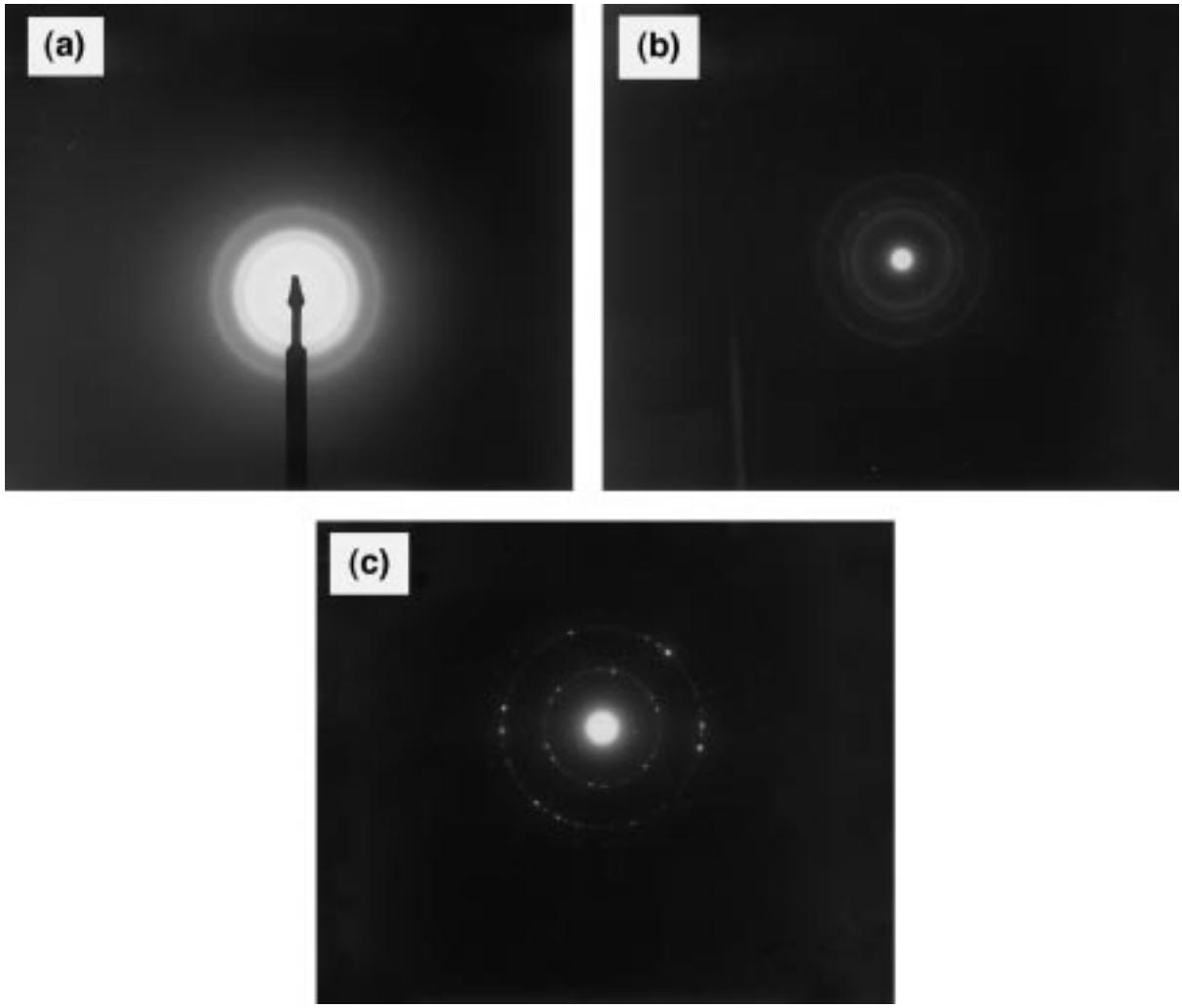

Fig. 8. Electron diffraction patterns of the deposits shown in Figure 9. (a) pH 8.0; (b) pH 9.0; (c) pH 10.0.

patterns of the alloys obtained at pH 10.0 and pH 11.2 are similar (Fig. 8(c)) and show sharp and continuous rings with intense spots inside. These results indicate a gradual change from a prevalently amorphous alloy with few and small crystallites (Fig. 8(a)) to a prevalently crystalline one, with different crystallite sizes (Fig. 8(c)).

The substantial decrease in phosphorus incorporated inside the alloys is responsible for the increase in average size of the crystallites [24]. This is in agreement with other works on the nucleation and growth of electroless Co–P, Ni–Co–P and Ni–P [14, 25] alloy deposits. The authors pointed out that the degree of alloys crystallinity strongly depends on their phosphorus content: the decrease in phosphorus content with pH leads to an increase in the average size of crystallites.

It is worth mentioning that the bath alkalinity affects only the sharpness of the TEM diffraction rings and not their positions. The crystalline phase present in the electroless Ni–Zn–P alloy was identified by calculating the interplanar distances from the diffraction patterns. Table 1 shows the d_{hkl} values calculated from Figure 8(c) and those tabulated for the f.c.c. nickel structure. The strong correlation demonstrates that the crystallites present in the alloys have the f.c.c. nickel structure. This was also found by other authors for electroless Ni–Zn–P thin films having Zn < 13 at % (a/o), which were prepared on activated substrate from a chloride bath [19].

Figure 9 shows the electron TEM image (Fig. 9(a)) and the corresponding electron diffraction pattern (Fig. 9(b)) of Ni–Zn–P alloy electrolessly deposited at pH 10.0 with a higher zinc concentration in the solution

Table. 1. Comparison among the interplanar distances measured (d_m) for the Ni–Zn–P alloy deposited at pH 10.0 and those tabulated for Ni (d_t)

N	$d_m \pm \Delta d_m$/Å	d_t (Ni)/Å	(h k l)
1	2.04 ± 0.04	2.03	(1 1 1)
2	1.72 ± 0.04	1.76	(2 0 0)
3	1.21 ± 0.04	1.24	(2 2 0)
4	1.02 ± 0.02	1.02	(2 2 2)
5	0.79 ± 0.02	0.79	(4 2 0)

(Zn^{2+} 0.05 M): crystallites 85 Å in size are present (Fig. 9(a)). The comparison with the crystals size of the deposit obtained at pH 10 with a lower Zn concentration in solution (0.01 M, Fig. 7(c)) shows that the increase in zinc content leads to a decrease in crystallites size. The electron diffraction pattern (Fig. 9(b)) shows continuous rings corresponding to f.c.c. nickel; therefore the increase in the deposit zinc content up to 23% does not change the nickel crystalline structure. These results suggest that both phosphorus and zinc are interstitial in the f.c.c. nickel attice.

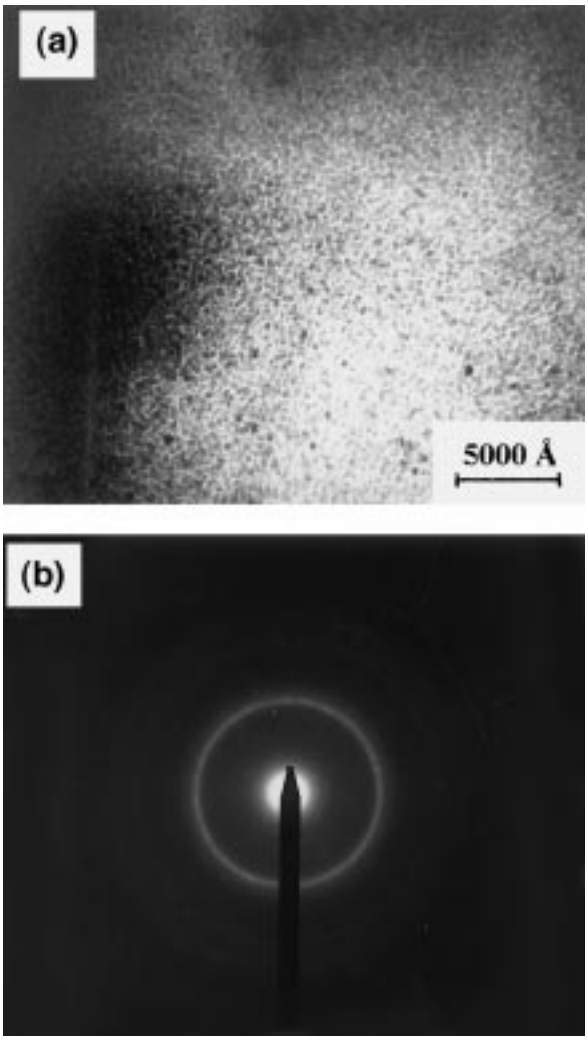

Fig. 9. Ni–Zn–P coating deposited from the solution with 0.05 M in zinc at pH 10.0. (a) TEM image, (b) electron diffraction pattern at higher magnification than those in Figure 8.

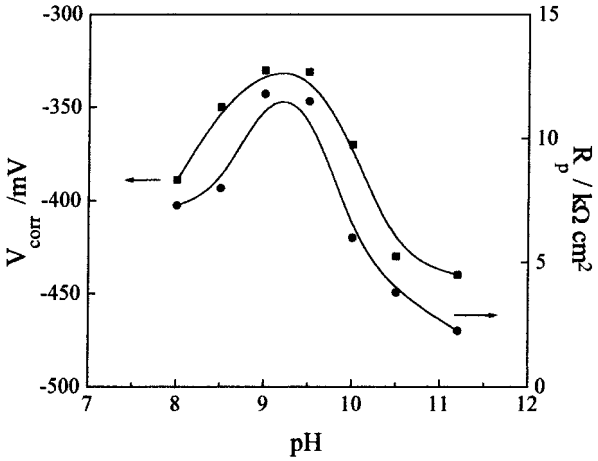

Fig. 10. Effect of bath pH on the corrosion potential and polarization resistance of electroless Ni–Zn–P alloy coatings in quiescent aerated 3% NaCl solution.

3.4. *Corrosion resistance*

Corrosion potential and polarization resistance values of electroless Ni–Zn–P alloys, deposited at different pH and immersed in quiescent aerated 3% NaCl solution, are shown in Figure 10. The change in pH strongly

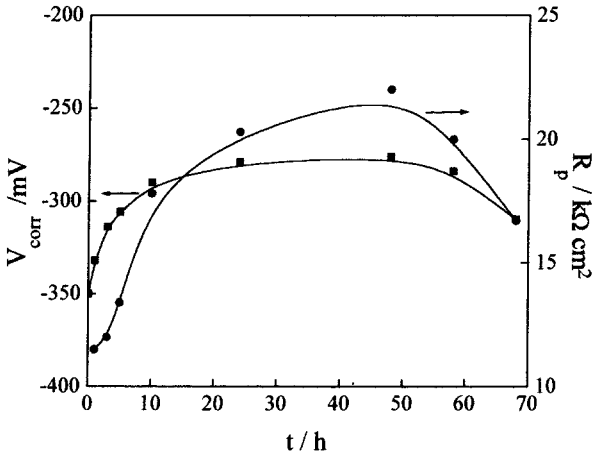

Fig. 11. Effect of immersion time in quiescent aerated 3% NaCl solution on the corrosion potential and polarization resistance values of Ni–Zn–P alloy coating obtained from the basic bath.

affects the corrosion potential values, which are more positive than those of the iron substrate (−476 mV vs SCE). E_{corr} increases up to pH 9.5 followed by a decrease and shift toward the substrate potential; the deposits obtained at pH values between 8.5–9.5 have a corrosion potential slightly lower than that measured on pure nickel (−271 mV), according to the high nickel content of the alloys. The trend in the polarization resistance values confirms the corrosion potential measurements: the deposits obtained at pH between 9.0–9.5, with a zinc and phosphorous content of 11.4–12.5% and 11.8–11.2%, respectively, show better corrosion resistance than those obtained at low or high pH. According to the SEM observations (Fig. 4(d)), the drop in corrosion resistance for the deposits obtained at pH above 10 is due to the cracks. The low corrosion resistance for the deposits obtained at pH 8.0 with a characteristic amorphous structure, can be attributed to the high phosphorous content, which makes it electrochemically active [19].

Figure 11 shows the effect of the time of immersion in 3% NaCl solution on the corrosion potential and polarization resistance values of the Ni–Zn–P deposit obtained from the basic bath at pH 9.0. At immersion, E_{corr} is about −350 mV; after about 20 h it stabilizes around −276 mV, corresponding to nickel oxides according to Pourbaix diagram [26]. This shift to more positive potentials is due to the formation of corrosion products which provide a diffusion barrier [19]. After about 60 h the potential decreases, indicating that the corrosion products are no longer protective.

4. Conclusions

The effect of pH on the morphology and microstructure of electrolessly deposited Ni–Zn–P alloys was studied using scanning electron microscopy, grazing incidence asymmetric Bragg X-ray diffraction and transmission electron microscopy. The results obtained are summarized as follows:

(i) SEM observations on the surfaces of electroless Ni–Zn–P alloys showed a morphological gradual change with bath pH. All the deposits are homogenous; at pH values > 8.0 rounded formations can be observed and at pH 11.2 the deposit is cracked and does not adhere to the iron substrate.

(ii) The grazing incidence asymmetric Bragg X-ray diffraction identified the coating as amorphous or microcrystalline.

(iii) TEM analysis confirmed the X-ray diffraction results. A transition from a prevalently amorphous to a polycrystalline alloy on increasing the bath pH was observed. The large decrease in phosphorus incorporated inside the deposits is responsible for this change. A single crystalline phase corresponding to f.c.c. nickel was found in the alloys obtained from strong alkaline solution. The increase in zinc content of the deposit up to 23% does not change the nickel crystalline structure. This indicates that both phosphorus and zinc are interstitial in f.c.c. nickel lattice.

(iv) Corrosion potential and polarization resistance values in quiescent aerated 3% NaCl solution showed that the electroless Ni–Zn–P alloy coatings, obtained at pH between 9.0–9.5 with a zinc and phosphorous content of 11.4–12.5% and 11.8–11.2%, respectively, have the best corrosion resistance.

Acknowledgements

The authors acknowledge the support of this work from European Community programme contract "N° 03/20/017 soutien à la recherche scientifique au Maroc".

References

1. E. Raub, *Plat. Surf. Finish.* **63** (1976) 29.
2. M. Ratzker, D.S. Lashmore and K.W. Pratt, *Plat. Surf. Finish.* **73** (1986) 74.
3. J. Crousier, Z. Hanane and J.P. Crousier, *Electrochim. Acta* **38** (1993) 261.
4. J.P. Bonino, S. Bruet-Hotellaz, C. Bories, P. Pouderoux and A. Rousset, *J. Appl. Electrochem.* **27** (1997) 1193.
5. A. Brenner and G.E. Riddell, *J. Res. Natl. Bur. Stand.* **37** (1946) 31; **39** (1947) 385.
6. G. Gutzeit, W.J. Crehan and A. Krieg, *UK Patent 761 556* (1957).
7. A. Brenner, *Metal Finish.* **52** (1954) 68.
8. ASTM, Special Technical Publication No. 265 (1959).
9. A.W. Goldenstein, W. Rostoker, F. Schossberger and G. Gutzeit, *J. Electrochem. Soc.* **104** (1957) 104.
10. A.H. Graham, R.W. Lindsay and H.J. Read, *J. Electrochem. Soc.* **112** (1965) 401.
11. M. Schlesinger and J.P. Marton, *J. Phys. Chem. Solids.* **29** (1968) 188.
12. J.P. Marton and M. Schlesinger, *J. Electrochem. Soc.* **115** (1968) 16.
13. R. Weil, J.H. Lee. I. Kim and K. Parker, *Plat. Surf. Finish.* **76** (1989) 62.
14. S.L. Chow, N.E. Hedgecock, M. Schlesinger and J. Rezek, *J. Electrochem. Soc.* **119** (1972) 1614.
15. S. Swathirajan and Y.M. Mikhail, *US Patent 4 758 479* (1988).
16. S. Swathirajan and Y.M. Mikhail, *J. Electrochem. Soc.* **136** (1989) 2188.
17. M. Schlesinger and D.D. Snyder, *US Patent 5 304 403* (19 Apr. 1994).
18. D.D. Snyder, M. Schlesinger and X. Meng, *J. Electrochem. Soc.* **137** (1990) 1858.
19. M. Schlesinger, X. Meng and D.D. Snyder, *J. Electrochem. Soc.* **138** (1991) 406.

20. M. Bouanani, F. Cherkaoui, M. Cherkaoui, S. Belcadi, R. Fratesi and G. Roventi, submitted to *J. Appl. Electrochem.*
21. J. Mindowicz, C. Capel-Boute and C. Decroly, *Electrochim. Acta* **10** (1965) 901.
22. M. Yunus, C. Capel-Boute and C. Decroly, *Electrochim. Acta*. **10** (1965) 885.
23. R. Fratesi, G. Roventi, G. Giuliani and C.R. Tomachuk, *J. Appl. Electrochem*. **27** (1997) 1088.
24. M. Bouanani, F. Cherkaoui, M. Cherkaoui, R. Fratesi and G. Roventi, Proceedings of the Second Mediterranean Basin Conference on 'Analytical Chemistry', Rabat, Morocco (23–28 Nov. 1997), p. PII–104.
25. P.A. Albert, F. Kovac, H.R. Lilienthal, T.R. McGuire, and Y. Nakamura, *J. Appl. Phys*. **38** (1967) 1258.
26. M. Pourbaix 'Atlas of Electrochemical Equilibria in Aqueous Solutions' (NACE, Houston, TX, 1974), p. 333.